Nanoscale

PAPER

View Article Online
View Journal | View Issue

Cite this: *Nanoscale*, 2018, **10**, 1038

Excitation wavelength dependent photon anti-bunching/bunching from single quantum dots near gold nanostructures†

Swayandipta Dey,[a] Yadong Zhou,[b] Yonglei Sun,[c] Julie A. Jenkins,[a] David Kriz,[a] Steven L. Suib,[a,c] Ou Chen,[d] Shengli Zou[b] and Jing Zhao*[a,c]

In this study, we aim to investigate the change in photon emission statistics of single CdSe/CdS core/shell quantum dots (QDs) on dielectric modified gold nanoparticle (NP) substrates as a function of the excitation wavelength. Photons emitted from single QDs are typically "anti-bunched" and are independent of the excitation wavelength. However, when QDs are coupled to plasmonic substrates, even at the low excitation power regime, we observed a significant change in photoluminescence emission behavior of single QDs; *i.e.* the emission transformed from incomplete photon anti-bunched to bunched when the excitation was changed from "off" to "on" plasmon resonance. Theoretical studies based on electrodynamics modeling suggested that for the QD–Au NP system, the quantum yield of single excitons decreases while that of biexcitons increases. In addition, when excited at the "on" resonance condition, the absorption is highly enhanced, resulting in an increased population of higher order excitons of the QDs. The higher order exciton emission was directly observed as an additional peak appeared at the blue side of the exciton peak of single QDs. The combined effect of the change in quantum yield and the increase in the absorption cross-section switches the photons emitted by single QDs from anti-bunched to bunched. These results provided direct evidence that not only the plasmonic nanostructures but also the excitation wavelength can effectively control the photon emission statistics of single QDs in the hybrid metal–semiconductor system. Manipulating the multiexciton–plasmon interaction in a hybrid complex like this could possibly open up new doors for applications such as entangled photon pair generation and plasmon-enhanced optoelectronic devices.

Received 20th July 2017,
Accepted 4th December 2017

DOI: 10.1039/c7nr05299e

rsc.li/nanoscale

Introduction

Colloidal quantum dots (QDs) have been under the spotlight of various research fields over the past few decades because of their unique light absorption and emission properties. In particular, the broad absorption and high photoluminescence (PL) quantum yield (QY) offered by QDs make them promising building blocks for light emitting devices,[1–5] and desirable fluorescent probes for biological imaging and tracking.[6–8] Nowadays, QDs with near-unity single exciton PL QY have been routinely synthesized owing to the advancement in the synthetic approaches of QDs. However, the PL QY of multiexcitons in typical QDs is often low due to the fast non-radiative Auger recombination,[9,10] limiting the applications of QDs in laser and quantum communication. An effective method to increase the multiexciton QY of QDs is to couple them to metal nanoparticles (MNPs).[11–15] The multiexciton emission of QDs can be enhanced when QDs are deposited on roughened gold and silver thin films,[11,13,16] as well as on silica-coated silver and gold nanoparticles (NPs).[12,17,18] This emission enhancement originates from the interaction of multiexcitons in QDs with the highly increased electric field around the MNPs, which is due to the excitation of localized surface plasmon resonance (LSPR) in the MNPs.[19,20] The exciton–plasmon interaction can even change the emitted photons of single QDs from anti-bunched to bunched.[13,21,22] Although a strong plasmonic effect on the radiative and non-radiative recombination of multiexcitons has been observed by several groups independently,

[a]*Department of Chemistry, University of Connecticut, 55 North Eagleville Rd, Storrs, CT, 06269-3060, USA. E-mail: jing.zhao@uconn.edu; Fax: +860-486-2981; Tel: +860-486-2443*
[b]*Department of Chemistry, University of Central Florida, 4111 Libra Drive, Orlando, Florida 32816-2366, USA*
[c]*Institute of Materials Science, University of Connecticut, Storrs, CT, 06269-3136, USA*
[d]*Department of Chemistry, Brown University, Providence, RI 02912, USA*

†Electronic supplementary information (ESI) available: Experimental details, calculations of $\langle N \rangle$ and $g_0^{(2)}$, additional blinking traces, $g^{(2)}(\tau)$ data, and PL spectra for single QDs on glass and near Au nanoparticles. See DOI: 10.1039/c7nr05299e

inconsistency exists in the literature about the multiexciton–plasmon interaction mechanism.[11,13,14,18,23,24] Moreover, since the electric field associated with a plasmon is highly dependent on the excitation wavelength, we expect that the excitation conditions will strongly impact the multiexciton–plasmon interaction and therefore the photon statistics of single QDs although for isolated QDs, their single or multi-exciton emission efficiency is nearly independent of the excitation wavelength. However, there is currently a lack of such studies.

Usually, photons emitted by a single QD are anti-bunched.[25] The degree of photon anti-bunching can be evaluated from the second-order photon intensity correlation histogram, $g^{(2)}(\tau)$. Under pulsed excitation, the relative area ratio of center ($\tau = 0$) to side (τ = time interval between pulses) peaks of $g^{(2)}(\tau)$, $g_0^{(2)}$, is a signature of the bunching/anti-bunching behavior of the emitted photons.[13,26–28] Moreover, when the excitation is at low pump fluence, the average photon absorbed per pulse $\langle N\rangle \rightarrow 0$, $g_0^{(2)}$ directly represents the ratio of biexciton QY to exciton QY, as reported by Nair *et al.*[26] This method has been applied in the previous studies on the multiexciton emission of single QDs near metal films or NPs.[11,13,29,30] However, when QDs are located close to MNPs, the absorption cross-section is greatly increased due to the enhanced electric field from plasmons, thus resulting in increased $\langle N\rangle$. Even though the pump power from the excitation source is maintained low, the probability of forming multiexcitons in QDs near MNPs is much higher than that of the isolated QDs. In this scenario, it becomes difficult to determine the biexciton QY of single QDs near MNPs without performing any population modeling.[13,26] Thus, the previous model of using the $g^{(2)}(\tau)$ function to calculate the biexciton QY of single QDs needs to be revisited for the QDs near MNPs.

In this work, we investigated how altering the excitation wavelength could promote the multiexciton emission of single QDs close to dielectric-modified Au NPs even under low excitation fluence. Surprisingly, by simply varying the excitation wavelength from "off" to "on" plasmon resonance, the photons emitted by single QDs near Au NPs changed from anti-bunched to bunched, which was not observed in QDs on glass substrates. To understand this phenomenon, we re-evaluated the relationship between the $g^{(2)}(\tau)$ function and the multiexciton emission QY of QDs in the hybrid QD–MNP system. Electrodynamics modeling was also applied to quantitatively determine the absorption and emission rates of single and biexcitons at "on" and "off" plasmon resonance conditions.

The system we studied is composed of individual CdSe/CdS core/shell QDs dispersed on a substrate of Au NPs coated with alumina. Fig. 1(A) shows the schematic representation of the substrate preparation. The Au NP substrates were fabricated by immobilizing 120 nm Au NPs on glass, following a previously developed protocol.[12,31–33] A 20 nm thick alumina layer was then grown over the Au NPs using atomic layer deposition (ALD) to prevent complete quenching of QD emission. CdSe/CdS core/shell QDs were synthesized following a previously reported method in the literature.[34] The QDs with a quantum yield of 95% in hexane were diluted and spun-cast onto the Au

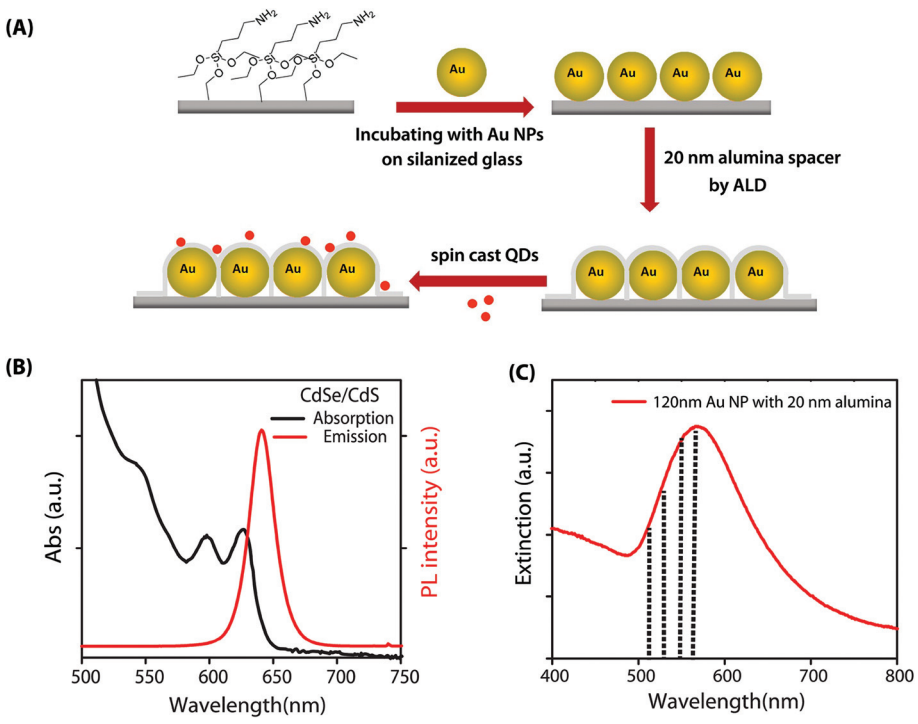

Fig. 1 (A) Schematic representation of substrate preparation for single QD optical measurements. (B) Absorption and emission spectra of CdSe/CdS QDs dispersed in hexane. (C) The extinction spectrum of 120 nm Au NPs with a 20 nm thick alumina spacer (dotted lines represent different excitation wavelengths used for the single particle studies at 510 nm, 530 nm, 550 nm and 580 nm).

NP–alumina substrate. The morphology of the QDs and alumina-coated Au NPs on glass can be determined from the transmission electron microscopy image and scanning electron microscopy image in Fig. S1 in the ESI.† Fig. 1(B) shows the absorption and PL spectra of the CdSe/CdS QDs dispersed in hexane. The absorption spectrum shows several distinct excitonic features associated with discrete electronic transitions in the QDs. The emission spectrum shows a narrow (FWHM ~ 21 nm) band-edge emission peak at 638 nm. The Au NP–alumina substrate has an LSPR peak at ~590 nm as shown in Fig. 1(C). The LSPR of the Au NPs has a substantial overlap with the PL spectrum of the QDs, leading to a strong exciton–plasmon interaction. The dotted lines on the extinction spectrum in Fig. 1(C) represent different laser excitation wavelengths (510, 530, 550 and 580 nm) used in our study.

To obtain the $g^{(2)}(\tau)$ function of the QDs as well as the PL intensity time traces, single QDs on the Au NP/alumina substrate were excited with a pump power of 50 nW at wavelengths of 510, 530, 550 and 580 nm. The value of $\langle N \rangle$ was found to be 0.045 for 510 nm, 0.027 for 530 nm, 0.023 for 550 nm, and 0.021 for 580 nm excitation. The calculation of $\langle N \rangle$ is available in the ESI.† To ensure that the QDs did not undergo photodegradation during the measurements, we varied the order of the excitation wavelength to which the QDs were exposed and no obvious difference in the PL intensity time trace was observed. Fig. 2 shows the $g^{(2)}(\tau)$ functions with the corresponding PL time traces for a single QD on Au NP substrates acquired at 510 nm, 530 nm, 550 nm and 580 nm excitation, respectively (also see additional data in Fig. S3†). The PL time traces show clearly binary-state (on and off) blinking, confirming that the signal is from a single QD. The PL intensity of the QD decreased on increasing the excitation wavelength in this case, because the absorbance of the QD is lower at 580 nm compared to 510 nm, and the exciton emission was quenched due to the Au substrate. However, for the $g^{(2)}(\tau)$ functions, there is a drastic increase of the relative size of the center peaks to the side peaks when the excitation wavelength was increased from 510 nm (off-resonance) to 580 nm (on-resonance). The high center peak of the $g^{(2)}(\tau)$ function shows that the multiexciton emission of QDs is highly enhanced when they are close to MNPs, consistent with previous reports.[11–13,18,35] Moreover, the intensity of the center peak became even higher than that of the side peak at 580 nm excitation. In contrast, in the control experiments performed on single QDs on glass (Fig. S2†), the $g^{(2)}(\tau)$ functions show no dependence on excitation wavelengths. In order to quantitatively evaluate the degree of enhancement of biexciton to exciton QY (η_{BX}/η_X) as a function of the excitation wavelength, we calculated the values of $g_0^{(2)}$ for 45 individual QDs collected on glass, and 38 QDs on Au NP substrates. Fig. 3 shows the box and whisker plots of $g_0^{(2)}$ at different excitation wavelengths. For the QDs on glass, $g_0^{(2)}$ shows a small dot-to-dot variation that is independent of the excitation wavelength. The average value of $g_0^{(2)}$ is 0.2, giving $\eta_{BX} \sim 0.2$ of single QDs on glass, according to the previous literature,[26,36] whereas for the QDs on Au substrates, the average value of $g_0^{(2)}$ increases from 0.62 (at 510 nm excitation) to 1.33 (at 580 nm excitation). The dot-to-dot variation in the values of $g_0^{(2)}$ is much larger in the QDs on the Au substrate than that of the QDs on glass. This is likely due to the variations in the positions of the QDs relative to Au NPs. Since η_{BX} and η_X are dependent on the distance between the QD and the Au NPs as reported in our previous studies,[12] the value of $g_0^{(2)}$ will depend on the location of the QDs on the Au substrate. Nevertheless, the results show that by varying the excitation wavelength from "off" to "on" plasmon resonance, the photons emitted by a QD near Au NPs change dramatically from anti-bunched to bunched. For the same QD near an MNP, its multiexciton emission can be easily controlled by changing the excitation wavelength.

The multiexciton emission intensity of QDs is dependent on the excitation power.[13,37,38] Thus, in order to further understand the effect of plasmons on single and multiexciton emission, we measured the $g^{(2)}(\tau)$ functions of QDs at varying pump power at 580 nm excitation both on glass and on Au substrates (Fig. S4†). We are particularly interested in this wavelength because it is in resonance with LSPR and the effect on enhancement in multiexciton emission is more pronounced. The excitation powers used in our study were 50 nW, 250 nW, 500 nW, 1000 nW, and 2500 nW. The estimated values of $\langle N \rangle$ for these powers are 0.02, 0.10, 0.21, 0.43, and 1.07, respectively (see the ESI† for the calculation of $\langle N \rangle$). The $g_0^{(2)}$ value as a function of the excitation power is plotted in Fig. 4. The average value of $g_0^{(2)}$ of the QDs on glass increases from 0.19 to 0.78 when the excitation power increases from 50 nW to 2500 nW, which is due to the excitation of more biexcitons at a higher power, whereas for the QDs on the Au substrate, the average value of $g_0^{(2)}$ is 1.16 at 50 nW excitation. The $g_0^{(2)}$ value increases gradually and levels off to 1.5 at 2500 nW excitation. This change in $g_0^{(2)}$ when increasing the pump power seems different from the previous results reported in ref. 13. The difference mainly lies in the different plasmonic structures employed in our work (Au NPs) and their work (roughened Ag films), where the enhancement in the electric field provided by the Au NPs at resonance excitation is much higher. The difference also arises because the emission of higher order multiexcitons (such as triexciton) is partly cut-off by the emission filter which we used to block the excitation light. In addition to $g^{(2)}(\tau)$ measurements, pump-power dependent single QD PL spectra were simultaneously recorded. Along with increased biexciton emission when increasing the excitation power, there is a red-shift in the peak position of the PL spectra for the QDs on glass of ~20 meV (Fig. 4B and S5-A†). The red-shift is due to the biexciton binding energy, as previously reported.[39–42] When the QDs were placed on Au substrates, an additional peak appeared at the blue (higher energy) side of the PL spectra along with the red shift of the band-edge emission peak (see Fig. 4D and Fig. S5-B†). Moreover, the intensity of the additional peak increases with increasing excitation power. We were not able to measure the complete peak feature because a 600 nm longpass emission filter was used to block the excitation laser light at 580 nm. The additional peak feature at ~600 nm is ascribed to the emission from higher

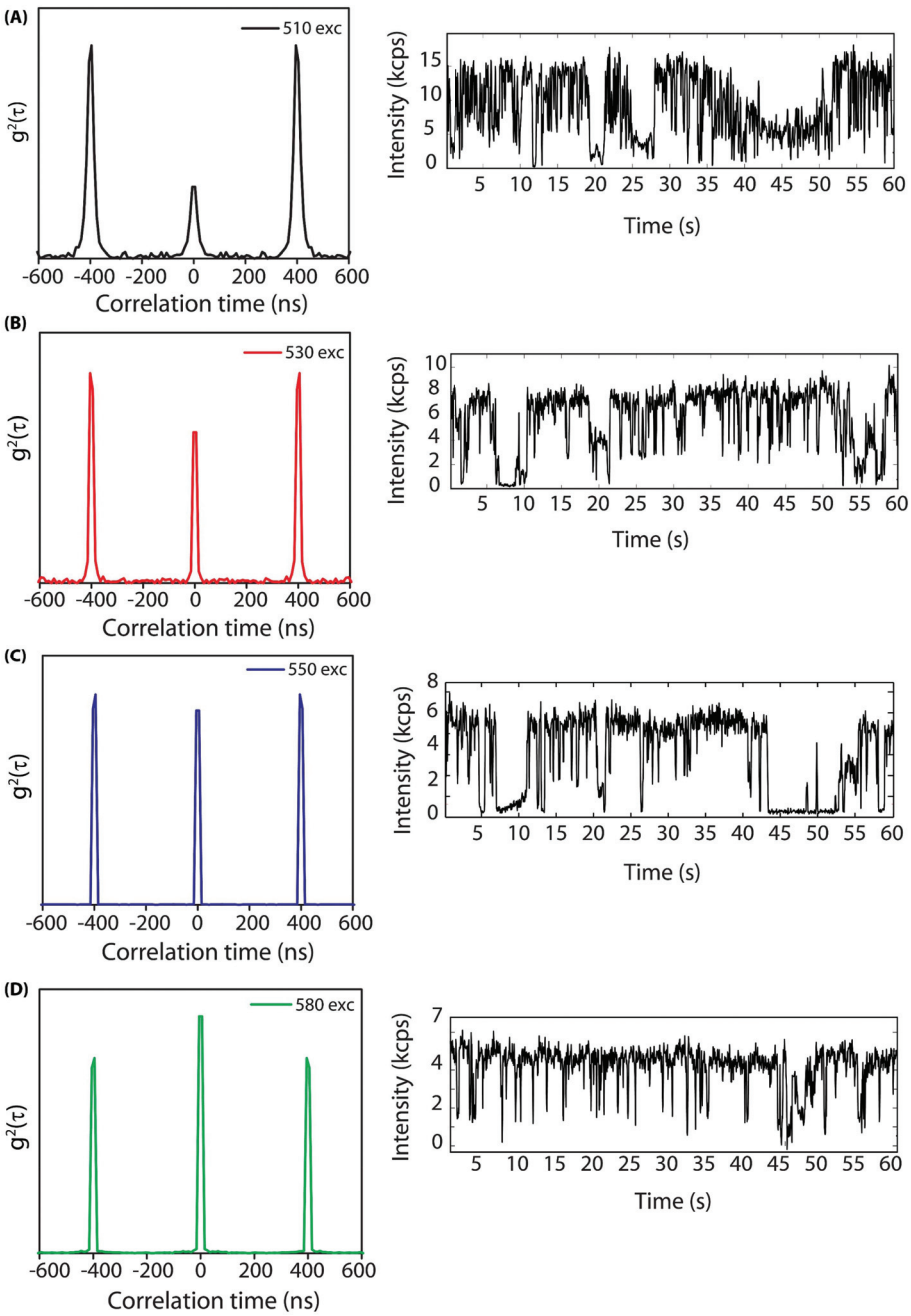

Fig. 2 Representative time-dependent second order photon intensity correlation functions ($g^{(2)}(\tau)$ functions) and the corresponding intensity–time traces of a single QD deposited on Au NPs with 20 nm alumina substrates at excitation wavelengths of (A) 510 nm, (B) 530 nm, (C) 550 nm and (D) 580 nm.

excitonic states, such as triexcitons of QDs. Triexciton emission was not observed in the QDs on glass because triexcitons could not be populated at the excitation power used in the experiment. Only at a very high excitation power, the additional feature in the PL spectra of single QDs on glass was observed at the blue side of the band-edge emission peak (see Fig. S6†). But when QDs were close to Au NPs and excited at LSPR, their absorption cross-section was highly increased due to the plasmon resonance (see below for more discussion). This highly enhanced absorption makes it much easier to populate the higher order excitons in the QDs near Au NPs compared to the isolated ones. Therefore, triexciton emission was observed for the QDs on Au but not on glass at the same laser power.

From the experiments, we found that the multiexciton emission of QDs near Au NPs is highly dependent on the excitation wavelength. One important factor accounting for this excitation wavelength dependence is the difference in the QD

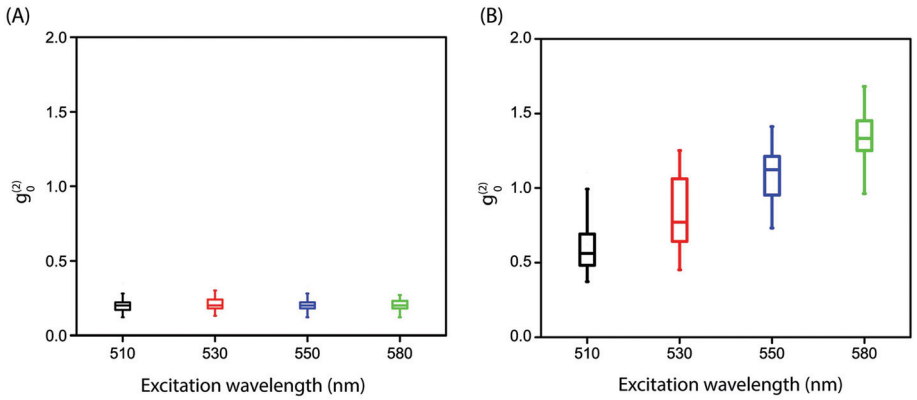

Fig. 3 Box and whisker plots representing the measured $g_0^{(2)}$ values (the integrated area ratio of the center to side peaks obtained from $g^{(2)}(\tau)$ functions) of single QDs excited at 510 nm (black), 530 nm (red), 550 nm (blue) and 580 nm (green). The single QDs were deposited on (A) glass and on (B) Au NP substrates. The lines inside the box indicate the median values, the box edges indicate the first and third quartiles, and the top and bottom lines represent the maximum and minimum values.

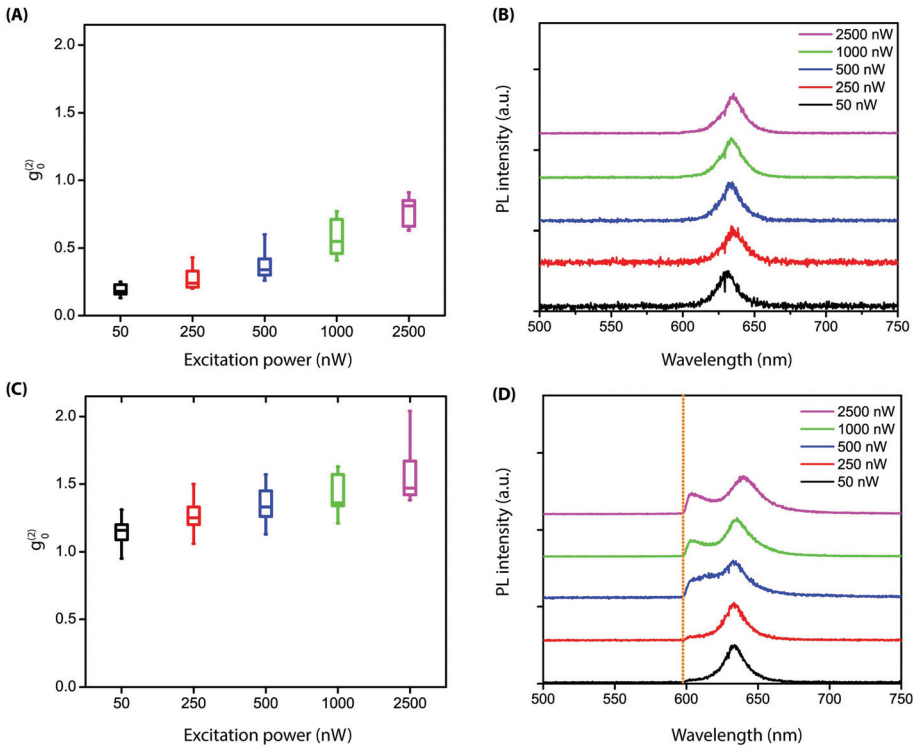

Fig. 4 Box and whisker plots representing the pump power dependence of $g_0^{(2)}$ values plotted as a function of the excitation power at 580 nm excitation for single QDs deposited on (A) glass and (C) Au NP substrates. (B) and (D) The representative photoluminescence spectra of a single QD on glass and on the Au NP substrate under 580 nm excitation at different excitation powers (50 nW, 250 nW, 500 nW, 1000 nW and 2500 nW). The dotted line in figure (D) indicates the 600 longpass emission filter.

absorption cross-section at different wavelengths. This hypothesis is based on the well-established fact that the excitation of LSPR results in a highly enhanced electric field around the MNP, the magnitude of which is dependent on the excitation wavelength.[43–45] To test our hypothesis, an electrodynamics simulation using the discrete dipole approximation method was performed to determine the change in the absorption cross-section of a single QD near Au NPs at different excitation wavelengths.[46] In the simulations, an 8 nm QD was placed next to a 120 nm Au sphere, separated by a 20 nm layer of alumina (see Fig. 6A for the scheme). The direction of the incident electric field was varied to be perpendicular or parallel to the axis defined by the center of the QD and the Au NP to account for the uncertainty in the direction of the electric field. The table in Fig. 6A shows the average electric field enhancement factor (EF). The enhancement factor EF is calculated using $\mathrm{EF} = |E|^2/|E_{\mathrm{inc}}|^2$,

where $|E|$ is the magnitude of the electric field the QD experiences, and $|E_{inc}|$ is the magnitude of the incident electric field. As a result of the electric field enhancement, the absorption cross-section of the QD near the Au NP is enlarged by EF times. The population of single and multiexcitons generated per pulse will change accordingly. Since the absorption of QDs follows the Poisson distribution, the probability of generating the k-th exciton is $P_{k\text{-th exciton}} = \frac{(\mathrm{EF} \times \langle N \rangle)^k \times e^{-\mathrm{EF} \times \langle N \rangle}}{k!}$, where k = 1 for a single exciton, and k = 2 for a biexciton and so on. Comparing the QDs on glass and on the Au substrate, P_{TX} is negligible for the QDs on glass at a low excitation power, but P_{TX} is much higher for the QDs on the Au substrate. That is the reason why the triexciton emission was observed in the QDs on the Au NP substrate but not in the QDs on glass at the same laser power (Fig. 4B and D).

In addition to the absorption enhancement, the exciton/multiexciton decay dynamics and QYs of QDs are also modified when they are situated close to an MNP. Fig. 5 compares the PL decay of a single QD on glass (Fig. 5A) and close to Au NPs (Fig. 5B) when the excitation wavelength was varied. It is evident that the PL decay of the QD on glass is independent of the excitation wavelength. Surprisingly, the PL decay of a single QD close to Au NPs changes upon changing the excitation wavelength. This phenomenon was observed in a few previous studies on QDs near metal NPs, but the mechanism is still unclear.[47,48] One possible reason that could contribute to the PL decay change is that new emitting species with faster PL decay rates may form at the excitation wavelength close to the plasmon resonance of the Au NPs. To examine this possibility, the PL spectra of the hybrid system at different excitation wavelengths were recorded, but no significant changes were observed in the spectra. Therefore, we do not have any evidence that any new emitting species with different PL lifetimes were formed when varying the excitation wavelength. The change in the PL decay is possibly due to the higher multiexciton emission at 580 nm excitation than at 510 nm. Since the multiexciton lifetime is much shorter than the single exciton lifetime, the PL decay of the hybrid system QD becomes faster when there is a larger contribution from multiexciton emission in the PL. This is consistent with the "bunching" of photons we observed when the system was excited close to the plasmon resonance. Now we discuss the change in the QYs of the QDs when they are close to Au NPs. For an isolated QD, its emission QY can be expressed as $\eta = \frac{k_r}{k_r + k_{nr}}$, where k_r and k_{nr} are the intrinsic radiative and non-radiative recombination rates of the QD. When the QD is placed near an MNP, its QY is modified and the new QY can be calculated with the following equation: $\eta' = \frac{k'_r}{k'_r + k_{nr} + k_{ET}}$, where k'_r is the modified radiative rate and k_{ET} is the additional non-radiative energy transfer rate from the QD to the MNP. Using these equations, the exciton and biexciton QYs of a QD close to the Au NP (as illustrated in the scheme in Fig. 6A) were calculated for the scenario when the electric field was perpendicular or parallel to the axis defined by the centers of the QD and the Au NP. The averaged η'_X for single exciton is calculated to be 0.54 and the averaged η'_{BX} for biexciton is 0.36. The η'_X (= 0.54) value is lower than η_X (= 0.95), meaning that the PL of excitons is partially quenched when the QD was close to the 120 nm Au NP. In contrast, η'_{BX} (= 0.36) is higher than η_{BX} (= 0.2), showing that the PL of biexcitons is enhanced in this case. This quenching/enhancing of exciton/biexciton emission in QDs near Au NPs has also been observed in our previous work.[12]

Using the modified QY and $\langle N \rangle_{eff}$ where $\langle N \rangle_{eff} = \langle N \rangle \times \mathrm{EF}$, the value of $g_0^{(2)}$ was calculated using $g_0^{(2)} = \frac{2P_{\langle N \rangle_{eff \geq 2}}}{\left(P_{\langle N \rangle_{eff \geq 1}}\right)^2} \frac{\eta'_{BX}}{\eta'_X}$ as a function of $\langle N \rangle_{eff}$ and the results are shown in Fig. 6B (see the detailed derivation in the ESI†). According to the calculation, $g_0^{(2)}$ increases with increasing $\langle N \rangle_{eff}$ and levels off, consistent with the experimental observations in Fig. 4. In particular, when $\langle N \rangle_{eff}$ is greater than 1.6, the $g_0^{(2)}$ value increases to above 1, indicating that the bunching of the observed emitting photons can be achieved under such conditions. To understand the excitation wavelength dependence of $g_0^{(2)}$, $\langle N \rangle_{eff}$ is calculated for 510, 530, 550 and 580 nm excitation at 50 nW power using the $\langle N \rangle$ of the QD at these wavelengths and the average EF listed in Fig. 6A. The average EF is calculated by averaging the electric field obtained when the incident polarization is perpendicular or parallel to the axis defined by the

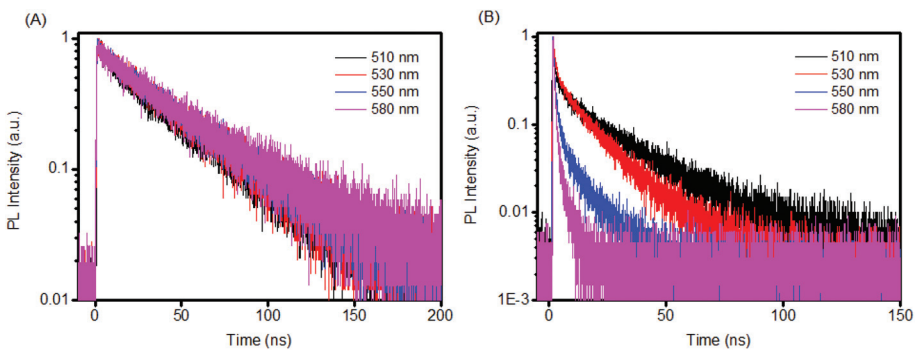

Fig. 5 Excitation wavelength dependent PL decay for a single QD (A) on glass and (B) on the Au NP substrate.

(A)

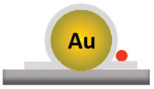

Excitation wavelength (nm)	Average enhancement factor
510 nm	2.5
530 nm	3.2
550 nm	5.2
580 nm	11.9

(B)

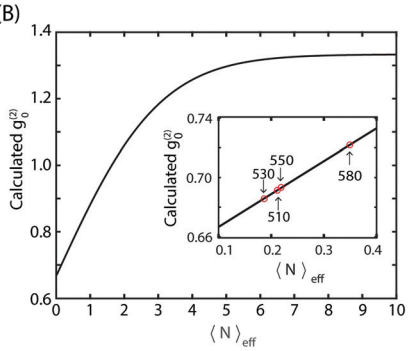

Fig. 6 (A) The table indicates the calculated enhancement factors obtained at different excitation wavelengths for a single QD positioned on an Au NP substrate. The enhancement factor (EF = $|E|^2/|E_{inc}|^2$) is averaged considering the variation in the electric field direction. (B) A plot of the calculated $g_0^{(2)}$ values against $\langle N \rangle_{eff}$.

centers of the Au NP and the QD. In the inset of Fig. 6B, the $g_0^{(2)}$ values of a QD near an Au NP for 510, 530, 550 and 580 nm excitation wavelengths are labeled. The $g_0^{(2)}$ values are lower than the experimental data (shown in Fig. 3), and $g_0^{(2)}$ at 530 nm is lower than $g_0^{(2)}$ at 510 nm. This discrepancy is likely because we underestimated the EF. Since the Au NPs are not exactly spherical in shape but are rather ellipsoidal (see the SEM image in Fig. S1-B†), the EF of an ellipsoidal particle is expected to be higher than the EF of the spherical particle with a similar diameter.[45] This model does not include the contribution of the emission from higher order excitons, *i.e.*, triexciton and above. We cut off the terms of higher order exciton emission because in the experiment, some of the emitted photons from high order exciton recombination were not collected (see detailed discussion in the ESI†). It is acceptable to do so when the laser power is low and the EF is moderate. But at a high laser power, there is substantial emission from triexcitons or even higher order excitons (*e.g.* Fig. 4D). The emission from higher order excitons should not be neglected in that case. Photon-induced charging can modify the photon statistics too.[13] In the previous analysis, we assume that all the single QDs are neutral. However, single QDs exhibit different PL decay dynamics when they are near Au NPs, which were not seen when on glass substrates (see Fig. 5). This indicates that the photon-induced charging could occur in the QDs near Au NPs.[49] According to the previous study,[13] we expect a slightly different degree of bunching in neutral QDs than we observed in our experiment. Nevertheless, we show both experimentally and theoretically that the $g_0^{(2)}$ of a QD near Au NPs is dependent on the excitation wavelength and also on the excitation power.

In conclusion, the photon emitting behavior of single QDs can be manipulated by placing the QDs near plasmonic structures and varying the excitation wavelength. This effect of exciton conditions was demonstrated in a simple hybrid system consisting of single CdSe/CdS QDs near Au NPs. Specifically, the photons emitted by a single QD switched from incomplete "anti-bunched" to "bunched" when the hybrid system was excited "on" plasmon resonance compared to "off" resonance. In contrast, photons emitted by single QDs on glass are usually anti-bunched and independent of the excitation wavelength. The results suggest that excitation conditions should be considered when designing strongly coupled exciton–plasmon systems for optoelectronic devices or lasers.

Author contributions

The manuscript was written through contributions of all authors. All authors have given approval to the final version of the manuscript.

Funding sources

NSF CHE# 1554800. DOE DE-FG02-86ER13622.A000.

Conflicts of interest

There are no conflicts to declare.

Acknowledgements

We would like to acknowledge financial support from National Science Foundation CAREER AWARD (CHE# 1554800). SLS acknowledges the US Department of Energy, Office of Basic Energy Sciences, Division of Chemical, Biological and Geological Sciences under grant DE-FG02-86ER13622.A000 for support of this research.

References

1 L. Qian, Y. Zheng, J. Xue and P. H. Holloway, *Nat. Photonics*, 2011, **5**, 543–548.
2 Q. Sun, Y. A. Wang, L. S. Li, D. Wang, T. Zhu, J. Xu, C. Yang and Y. Li, *Nat. Photonics*, 2007, **1**, 717–722.
3 X. Dai, Z. Zhang, Y. Jin, Y. Niu, H. Cao, X. Liang, L. Chen, J. Wang and X. Peng, *Nature*, 2014, **515**, 96–99.
4 B. S. Mashford, M. Stevenson, Z. Popovic, C. Hamilton, Z. Zhou, C. Breen, J. Steckel, V. Bulovic, M. Bawendi, S. Coe-Sullivan and P. T. Kazlas, *Nat. Photonics*, 2013, **7**, 407–412.
5 Y. Shirasaki, G. J. Supran, M. G. Bawendi and V. Bulovic, *Nat. Photonics*, 2013, **7**, 13–23.
6 X. Michalet, F. F. Pinaud, L. A. Bentolila, J. M. Tsay, S. Doose, J. J. Li, G. Sundaresan, A. M. Wu, S. S. Gambhir and S. Weiss, *Science*, 2005, **307**, 538.
7 M. Howarth, W. Liu, S. Puthenveetil, Y. Zheng, L. F. Marshall, M. M. Schmidt, K. D. Wittrup, M. G. Bawendi and A. Y. Ting, *Nat. Methods*, 2008, **5**, 397–399.
8 K. D. Wegner and N. Hildebrandt, *Chem. Soc. Rev.*, 2015, **44**, 4792–4834.
9 J. M. Caruge, Y. Chan, V. Sundar, H. J. Eisler and M. G. Bawendi, *Phys. Rev. B: Condens. Matter*, 2004, **70**, 085316.
10 V. I. Klimov, A. A. Mikhailovsky, D. W. McBranch, C. A. Leatherdale and M. G. Bawendi, *Science*, 2000, **287**, 1011.
11 S. J. LeBlanc, M. R. McClanahan, M. Jones and P. J. Moyer, *Nano Lett.*, 2013, **13**, 1662–1669.
12 S. Dey, Y. Zhou, X. Tian, J. A. Jenkins, O. Chen, S. Zou and J. Zhao, *Nanoscale*, 2015, **7**, 6851–6858.
13 Y.-S. Park, Y. Ghosh, Y. Chen, A. Piryatinski, P. Xu, N. H. Mack, H.-L. Wang, V. I. Klimov, J. A. Hollingsworth and H. Htoon, *Phys. Rev. Lett.*, 2013, **110**, 117401.
14 S. Masuo, K. Kanetaka, R. Sato and T. Teranishi, *ACS Photonics*, 2016, **3**, 109–116.
15 F. Wang, N. S. Karan, H. Minh Nguyen, Y. Ghosh, J. A. Hollingsworth and H. Htoon, *Sci. Rep.*, 2015, **5**, 14313.
16 D. Canneson, I. Mallek-Zouari, S. Buil, X. Quélin, C. Javaux, B. Mahler, B. Dubertret and J. P. Hermier, *Phys. Rev. B: Condens. Matter*, 2011, **84**, 245423.
17 H. Naiki, A. Masuhara, S. Masuo, T. Onodera, H. Kasai and H. Oikawa, *J. Phys. Chem. C*, 2013, **117**, 2455–2459.
18 H. Naiki, T. Uedao, L. Wang, N. Tamai and S. Masuo, *ACS Omega*, 2017, **2**, 728–737.
19 M. T. Achermann, *J. Phys. Chem. Lett.*, 2010, **1**, 2837–2843.
20 S. Dey and J. Zhao, *J. Phys. Chem. Lett.*, 2016, **7**, 2921–2929.
21 F. Jahnke, C. Gies, M. Aßmann, M. Bayer, H. A. M. Leymann, A. Föerster, J. Wiersig, C. Schneider, M. Kamp and S. Höfling, *Nat. Commun.*, 2016, **7**, 11540.
22 A. J. Bennett, J. P. Lee, D. J. P. Ellis, T. Meany, E. Murray, F. F. Floether, J. P. Griffths, I. Farrer, D. A. Ritchie and A. J. Shields, *Sci. Adv.*, 2016, **2**, e1501256.
23 H. Naiki, S. Masuo, S. Machida and A. Itaya, *J. Phys. Chem. C*, 2011, **115**, 23299–23304.
24 K. Matsuzaki, S. Vassant, H.-W. Liu, A. Dutschke, B. Hoffmann, X. Chen, S. Christiansen, M. R. Buck, J. A. Hollingsworth, S. Götzinger and V. Sandoghdar, *Sci. Rep.*, 2017, **7**, 42307.
25 P. Michler, A. Imamoglu, M. D. Mason, P. J. Carson, G. F. Strouse and S. K. Buratto, *Nature*, 2000, **406**, 968–970.
26 G. Nair, J. Zhao and M. G. Bawendi, *Nano Lett.*, 2011, **11**, 1136–1140.
27 S. Masuo, T. Tanaka, S. Machida and A. Itaya, *J. Photochem. Photobiol., A*, 2012, **237**, 24–30.
28 C. T. Yuan, P. Yu, H. C. Ko, J. Huang and J. Tang, *ACS Nano*, 2009, **3**, 3051–3056.
29 Y.-S. Park, Y. Ghosh, P. Xu, N. H. Mack, H.-L. Wang, J. A. Hollingsworth and H. Htoon, *J. Phys. Chem. Lett.*, 2013, **4**, 1465–1470.
30 T. B. Hoang, G. M. Akselrod and M. H. Mikkelsen, *Nano Lett.*, 2016, **16**, 270–275.
31 J. Kimling, M. Maier, B. Okenve, V. Kotaidis, H. Ballot and A. Plech, *J. Phys. Chem. B*, 2006, **110**, 15700–15707.
32 N. G. Bastús, J. Comenge and V. Puntes, *Langmuir*, 2011, **27**, 11098–11105.
33 J. A. Jenkins, Y. Zhou, S. Thota, X. Tian, X. Zhao, S. Zou and J. Zhao, *J. Phys. Chem. C*, 2014, **118**, 26276–26283.
34 O. Chen, J. Zhao, V. P. Chauhan, J. Cui, C. Wong, D. K. Harris, H. Wei, H.-S. Han, D. Fukumura, R. K. Jain and M. G. Bawendi, *Nat. Mater.*, 2013, **12**, 445–451.
35 H. Takata, H. Naiki, L. Wang, H. Fujiwara, K. Sasaki, N. Tamai and S. Masuo, *Nano Lett.*, 2016, **16**, 5770–5778.
36 J. Zhao, O. Chen, D. B. Strasfeld and M. G. Bawendi, *Nano Lett.*, 2012, **12**, 4477–4483.
37 H. Htoon, A. V. Malko, D. Bussian, J. Vela, Y. Chen, J. A. Hollingsworth and V. I. Klimov, *Nano Lett.*, 2010, **10**, 2401–2407.
38 D. Vanmaekelbergh, L. K. van Vugt, H. E. Bakker, F. T. Rabouw, B. d. Nijs, R. J. A. van Dijk-Moes, M. A. van Huis, P. J. Baesjou and A. van Blaaderen, *ACS Nano*, 2015, **9**, 3942–3950.
39 V. Klimov, S. Hunsche and H. Kurz, *Phys. Rev. B: Condens. Matter*, 1994, **50**, 8110–8113.
40 Y. Z. Hu, S. W. Koch, M. Lindberg, N. Peyghambarian, E. L. Pollock and F. F. Abraham, *Phys. Rev. Lett.*, 1990, **64**, 1805–1807.
41 K. I. Kang, A. D. Kepner, S. V. Gaponenko, S. W. Koch, Y. Z. Hu and N. Peyghambarian, *Phys. Rev. B: Condens. Matter*, 1993, **48**, 15449–15452.
42 B. O. Dabbousi, J. Rodriguez-Viejo, F. V. Mikulec, J. R. Heine, H. Mattoussi, R. Ober, K. F. Jensen and M. G. Bawendi, *J. Phys. Chem. B*, 1997, **101**, 9463–9475.
43 K. Tanabe, *J. Phys. Chem. C*, 2008, **112**, 15721–15728.
44 A. Agrawal, I. Kriegel and D. J. Milliron, *J. Phys. Chem. C*, 2015, **119**, 6227–6238.

45 E. Hao and G. C. Schatz, *J. Chem. Phys.*, 2004, **120**, 357–366.
46 B. T. Draine, *Astrophys. J.*, 1988, **333**, 848–872.
47 K. Munechika, Y. Chen, A. F. Tillack, A. P. Kulkarni, I. Jen-La Plante, A. M. Munro and D. S. Ginger, *Nano Lett.*, 2011, **11**, 2725–2730.
48 M. Focsan, A. M. Gabudean, A. Vulpoi and S. Astilean, *J. Phys. Chem. C*, 2014, **118**, 25190–25199.
49 C. Galland, Y. Ghosh, A. Steinbrück, J. A. Hollingsworth, H. Htoon and V. I. Klimov, *Nat. Commun.*, 2012, **3**, 908.